

## A numerical study of the genesis of concentric eyewalls in hurricanes

By SHANGYAO NONG\* and KERRY EMANUEL

*Massachusetts Institute of Technology, Cambridge, Massachusetts, USA*

(Received 30 July 2001; revised 11 April 2003)

### SUMMARY

We use two axisymmetric numerical models to explore the dynamics of concentric eyewalls in hurricanes. The first is a simple two-layer model using balanced dynamics and parametrized convection, while the second is a cloud-resolving non-hydrostatic model. In the case of the balanced model, infinitesimal disturbances amplify into secondary eyewalls provided the lower troposphere is sufficiently moist; otherwise, finite-amplitude perturbations are necessary to initiate amplifying structures. But experiments with the full-physics model show that finite-amplitude disturbances are always necessary to initiate secondary eyewalls, regardless of the initial humidity of the lower troposphere. Experiments with both models, in which the surface wind is held constant in the surface flux formulations, fail to develop secondary eyewalls, demonstrating that in these models the disturbances, once initiated, grow through the wind-induced surface heat exchange (WISHE) mechanism. Based on this work, we hypothesize that real secondary eyewalls result from a finite-amplitude WISHE instability, triggered by external forcing, such as interaction of the tropical cyclone with baroclinic eddies, topography, or local perturbations in sea surface temperature.

KEYWORDS: Eddy angular-momentum flux Tropical cyclogenesis WISHE

### 1. INTRODUCTION

A number of observational analyses (Willoughby *et al.* 1982, hereafter WCS82; Willoughby 1990; Black and Willoughby 1992) have shown that, during the development of some intense hurricanes, spiral bands form a partial or complete ring of heavy precipitation around the eyewall, and that such a ring usually contains a well-defined wind maximum. These inner and outer convective rings are generally referred to as concentric eyewalls. Hurricanes with concentric eyewalls often undergo characteristic intensity changes. As the outer eyewall contracts and intensifies, the hurricane stops intensifying and starts to weaken, i.e. the central pressure rises, the maximum tangential wind decreases, and the eyewall's radius increases. Some time later, the outer eyewall replaces the inner one and becomes the new primary eyewall. After an eyewall succession, hurricanes may resume intensification if conditions are otherwise favourable. For example, Hurricane Allen of 1980 had three separate concentric eyewall periods (WCS82). During these three cycles intensity the central pressure fell by more than 50 mb, along with scattered periods of weakening.

Several mechanisms have been proposed for the genesis of concentric eyewalls in hurricanes. WCS82 linked the genesis of outer eyewalls to spiral rainbands. The observational study by Samsury and Zipser (1995) showed that some, but not all, spiral rainbands are associated with wind maxima. The definition of a secondary eyewall requires the coexistence of a local rainband and secondary outer wind maxima, so that not all spiral rainbands may develop into secondary eyewalls. The study by Black and Willoughby (1992) suggests that some concentric eyewalls may have asymmetric precursors. WCS82 also proposed that the genesis of secondary eyewalls might be a consequence of symmetric instability occurring at the bottom of the outflow layer. But observational studies (Riehl 1979; Molinari and Vollaro 1990, hereafter MV90) found that

\* Corresponding author: MIT Rm. 54–1611, 77 Mass. Ave., Cambridge, MA, 02139, USA.

e-mail: snong@alum.mit.edu

© Royal Meteorological Society, 2003.

symmetric instability rarely occurs in the outflow layer. WCS82 went on to suggest that the downdraught surrounding the eye brings down low-momentum air, which induces a saddle in the wind profile. Willoughby *et al.* (1984), Lord *et al.* (1984) and Craig (1996) suggested that ice microphysical processes may be linked to the formation of concentric eyewalls. All tropical cyclones involve the ice phase, but not all such storms produce concentric eyewalls. Hawkins (1983) proposed that some concentric eyewalls that form in storms near shore are topographically forced. Of course, this idea cannot explain concentric eyewall formation in storms not influenced by land.

Montgomery and Kallenbach (1997) hypothesized that the formation of secondary eyewalls is due to the interaction between the basic vortex and vortex Rossby waves arising from moist convective forcing. This interaction was shown to accelerate the mean tangential winds and thus cause either genesis or intensity change. Camp and Montgomery (2001) further elaborated on this idea by adding a secondary vorticity ring to the developing vorticity field of an axisymmetric storm, which produced a concentric eyewall replacement cycle. It is possible that asymmetric dynamical processes intrinsic to the hurricane vortex, such as vortex axisymmetrization, may contribute to the genesis of concentric eyewalls. Notwithstanding these observations, this paper examines the dynamics of axisymmetric concentric eyewall cycles in the context of axisymmetric models.

Currently, the skill of hurricane intensity change forecasting is poor (DeMaria *et al.* 1993). Understanding the initial formation and development of outer eyewalls should shed light on the intensity changes associated with concentric eyewall cycles. Previous observational studies of tropical cyclones (Shapiro and Willoughby 1982; WCS82; Willoughby *et al.* 1984; Willoughby 1988) have shown that a large fraction of intensity changes are preceded by changes in eyewall radius or by formation of a secondary wind maximum outside the original eyewall. For example, Hurricane Andrew of 1992 almost regained its original peak intensity just before landfall after an eyewall replacement cycle. It was conjectured that the destructiveness of Andrew was related to the timing of the eyewall replacement (Willoughby and Black 1996).

In their observational studies of Hurricane Allen of 1980 and Hurricane Elena of 1985, Molinari and Vollaro (1989, 1990, 1992) and Molinari *et al.* (1995) suggested that convergence of upper-tropospheric eddy angular-momentum flux plays an important role in the intensity changes of these two hurricanes. In their study, Molinari and Vollaro (1989) showed that the development of Elena's secondary eyewall correlated at 30 hours lag with an increased inward flux of upper-level eddy angular momentum.

Inspired by these observations, we employ two numerical models to study the effect of environmental forcing on the genesis of concentric eyewalls. The models are the simple axisymmetric model developed by Emanuel (1989, 1995, hereafter E89, E95), and the axisymmetric, non-hydrostatic model developed by Rotunno and Emanuel (1987, hereafter RE87). Here we propose that an upper-tropospheric trough or other environmental perturbation induces an initial surface wind disturbance in the extant hurricane. If this disturbance becomes strong enough, and the environmental conditions are still favourable for further development, the disturbance triggers the formation of a secondary eyewall and the surface circulation amplifies through the wind-induced surface heat exchange (WISHE) mechanism of Emanuel (1989, 1993).

The organization of this paper is as follows. In the next two sections, the 'simple' and 'full-physics' models will be described and their results discussed. In the last section, concluding remarks will be presented.

## 2. RESULTS USING THE SIMPLE MODEL

(a) *The simple model*

The subcloud layer is assumed to be nearly in thermodynamic equilibrium, with sea surface fluxes nearly balancing the fluxes from convective updraughts and downdraughts and turbulence through the top of the subcloud layer. The rest of the troposphere is assumed to be in hydrostatic and gradient wind balance. The free atmosphere is also assumed to be neutral to slantwise moist convection, a condition approximated by constant saturation entropy along angular-momentum surfaces above the subcloud layer. The humidity of the free troposphere is described using only two layers.

The model is axisymmetric with potential radius  $R$  as the horizontal coordinate and pressure  $P$  as the vertical coordinate;  $R$  is proportional to the absolute angular momentum per unit mass surrounding the storm centre:

$$\frac{f}{2}R^2 \equiv rv + \frac{f}{2}r^2, \quad (1)$$

where  $f$  is the Coriolis parameter (assumed constant),  $r$  the physical radius from the storm centre and  $v$  the azimuthal velocity;  $R$  is the radius at which a parcel would attain zero azimuthal velocity if displaced radially away from the storm's centre while conserving angular momentum.

The numerical calculations of the model are performed in non-dimensional units. The primary scaling parameter is a measure of the atmosphere–ocean thermodynamic disequilibrium:  $\chi_s \equiv (T_s - T_t)(S_o^* - S_a)$  where  $T_s$  is the sea surface temperature,  $T_t$  tropopause temperature,  $S_o^*$  the ambient ocean surface saturation entropy, and  $S_a$  the entropy of the ambient subcloud layer. More details of the model can be found in E89 and E95.

When an initial vertical disturbance is placed near the sea surface, Ekman pumping induces upward motion and adiabatic cooling near the vortex core. The initial convective clouds penetrate dry air and have low precipitation efficiency (LPE). The convective heating from the LPE clouds can only partially compensate the adiabatic cooling, and the precipitation-induced downdraughts associated with the LPE clouds deplete the subcloud-layer entropy near the vortex core by bringing down middle-tropospheric air with low entropy, so that convective neutrality can be maintained. As a result, the vortex core cools and the vortex decays. However, if the initial vortex is strong enough, its surface wind can generate large surface heat fluxes. The fluxes not only counter the initial decreasing tendency of subcloud-layer entropy but also reverse this tendency and increase the subcloud-layer entropy. The entropy of the mid-troposphere increases because of the upward flux of now-elevated subcloud-layer entropy by the convective clouds. This raises the humidity of the middle troposphere and increases the precipitation efficiency. As the middle troposphere moistens, the convective downdraughts do not deplete the subcloud-layer entropy to the same degree. The vortex core warms and the vortex amplifies.

(b) *Numerical experiments and results*

The physical parameters in our control simulation EX1 are the same as those in the control run of E95. The initial middle-tropospheric relative humidity,  $\mathcal{H}_m$ , is 60%. The initial vortex is the same as in the control run of E95; specifically, the radius of maximum wind is 60 km, the radius of vanishing wind is 400 km, and the maximum azimuthal wind is  $15 \text{ m s}^{-1}$ . Experimental designs are described in Table 1.

TABLE 1. DESCRIPTION OF EXPERIMENTS WITH THE SIMPLE HURRICANE MODEL

EX1	Control
EX2	$\mathcal{H}_m$ increased from 60% to 90% in the lower troposphere
EX3	Same as EX2 except that surface wind at 8 days is used in the calculations of surface entropy fluxes after 8 days
EX4	Same as EX1 except that Gaussian random perturbations with zero mean and standard deviation of 5 are instantly added to the surface entropy fluxes at 9.4 days in the entire model domain
EX5	Same as EX4 except that the random perturbations begin at 9.4 days and last 7.5 hours in the entire model domain

The value of the standard deviation is a non-dimensional number. The typical value of the surface entropy fluxes is  $2.34 \text{ W m}^{-2} \text{ K}^{-1}$  based on the parameter values given in E89 and E95.

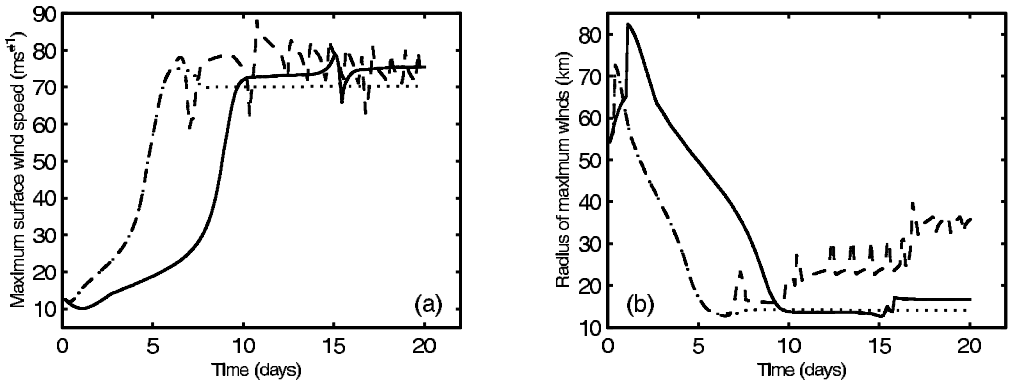


Figure 1. Time evolution of (a) maximum azimuthal surface wind and (b) radius of maximum wind of EX1 (solid line), EX2 (dashed line), and EX3 (dotted line).

Figure 1 shows the time evolution of maximum surface azimuthal wind  $v_{\max}$  and the radius of maximum wind  $r_{\max}$  for EX1, EX2 and EX3.

As seen in the Fig. 1, the model vortex in the control run EX1 evolves into a hurricane after 8 days, and reaches a steady state after 10 days. Numerical results indicate that only one eyewall\* formed during the whole integration time. The fluctuation at about 15 days does not involve any new eyewall formation.

In Experiment EX2, we increase the initial relative humidity of the middle troposphere. The time series of  $v_{\max}$  and  $r_{\max}$  from EX2 are shown in Fig. 1. Several significant fluctuations in the storm intensity seen in Fig. 1 are associated with eyewall replacement cycles. For example, the intensity fluctuations seen between 9 and 11 days, and between 16 and 18 days, are associated with eyewall replacement cycles. Here we analyse the intensity change between 9 and 11 days. Figure 2 shows vertical cross-sections of vertical velocity  $w$  at 10.11 and 10.225 days. The numerical results at 10.11 days indicate double surface wind maxima and double secondary circulations (figures not shown here). The fully developed inner eyewall (Fig. 2(a)) is about 20 km from the centre, while an outer eyewall has just appeared and is located about 50 km from the centre. At this time, the inner eyewall still dominates the outer eyewall. The outer eyewall propagates inwards and replaces the inner eyewall 12 hours later (Fig. 2(b)). This eyewall replacement process corresponds to the intensity change seen

\* Here and elsewhere we use the term 'eyewall' to denote a persistent vertical-velocity maximum.

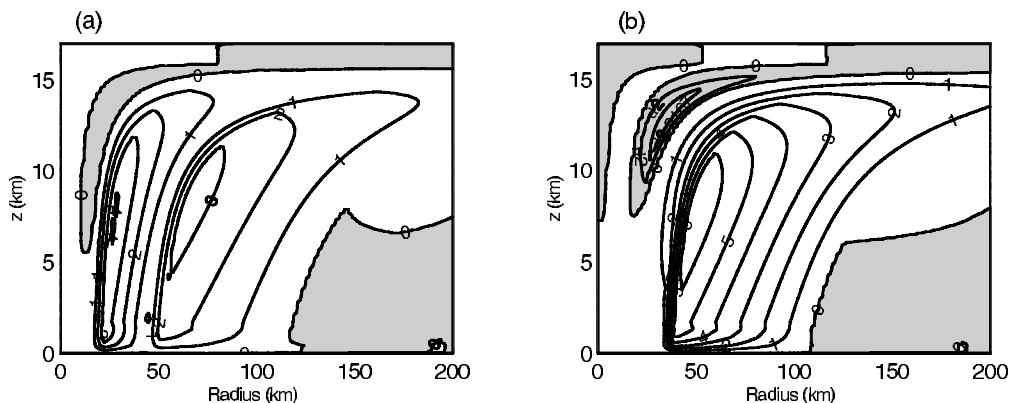


Figure 2. Vertical velocity of EX2 at (a) 10.11 days and (b) at 10.225 days. Negative values have been multiplied by 10 and shaded. Contour values are from  $-3$  to  $7$  at  $1 \text{ m s}^{-1}$  interval.

between 9 and 11 days in Fig. 1 (dashed line). Thus the simple model produces eyewall replacement cycles that resemble the observed ones described in the section 1.

Without the WISHE mechanism, however, concentric eyewalls do not develop in the model. The dotted lines in Fig. 1 are the time evolution of  $v_{\max}$  and  $r_{\max}$  in EX3. In this experiment, we use the surface wind at 8 days in the calculation of surface enthalpy fluxes after 8 days. By this means we turn off the positive feedback between the surface wind perturbations and surface enthalpy fluxes after 8 days. As shown in Fig. 1 (dotted line), the intensity reaches a steady state shortly after 8 days. The result of EX3 suggests that surface wind disturbances cannot be amplified without the WISHE mechanism.

To further assess the unstable nature of the concentric eyewalls, we performed two more numerical experiments in which Gaussian random perturbations were added to the surface enthalpy fluxes. Specifically, during the perturbation time period, the flux perturbations are drawn randomly from a Gaussian distribution of prescribed mean and standard deviation. Negative values are ignored. The results from these two experiments (see Table 1 for the difference between these two experiments) are shown in Fig. 3. There are no concentric eyewall cycles in EX4, while two full replacement cycles occur in EX5. We carried out more experiments to find the threshold values of the time duration and standard deviation of the random perturbations. We found that the time duration and the standard deviation should not be less than 5.7 hours and  $3.5^*$ , respectively, for the initial conditions of EX1. These values no doubt depend on the initial conditions and physical parameters of the control run EX1.

### (c) Conclusions from the simple model

Based on the numerical experiments with the simple model, we draw these conclusions:

(i) If the middle troposphere is moist enough, the simple model is able to produce concentric eyewalls without external forcing. The concentric eyewalls resemble those in nature.

(ii) The WISHE mechanism is responsible for the development of secondary eyewalls in the model.

\* This is a non-dimensional value. The typical value of the surface entropy fluxes is  $2.3 \text{ W m}^{-2} \text{ K}^{-1}$  based on the parameter values given in E89 and E95.

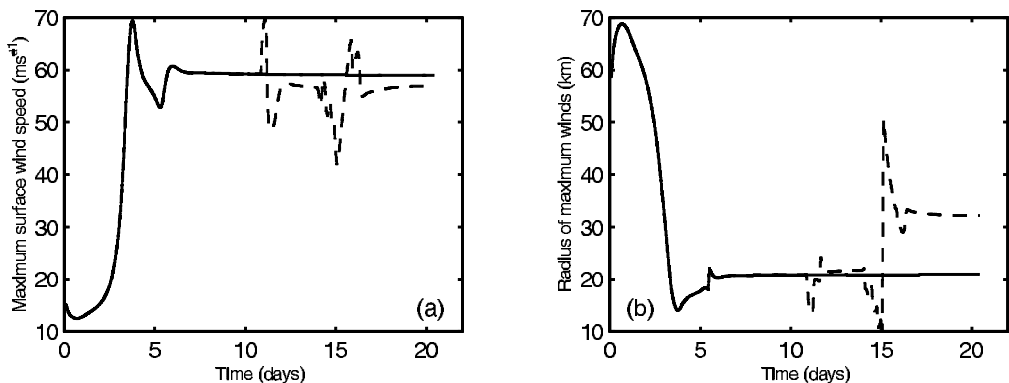


Figure 3. Time evolution of (a) maximum azimuthal surface wind and (b) radius of maximum wind of EX4 (solid line) and EX5 (dashed line).

(iii) If the lower troposphere is dry, an initial finite-amplitude disturbance is needed to trigger concentric eyewalls in the simple model.

### 3. RESULTS USING THE NON-HYDROSTATIC MODEL

#### (a) *The non-hydrostatic model and the parametrization of eddy forcing*

The non-hydrostatic model was originally developed by Rotunno and Emanuel (RE87) and revised by Bister (1996, hereafter B96). The model is an axisymmetric, cloud-resolving model with fully compressible, non-hydrostatic equations expressed in cylindrical coordinates. A detailed description of the model can be found in RE87 and B96.

We made two changes to the model to test the hypothesis we proposed in section 1. First, we implemented a very primitive ice scheme, to complement the Kessler-type warm-rain microphysics. Second, we added environmental forcing to the model.

To mimic one aspect of ice processes, we allow the terminal velocity,  $v_T$ , of rain to be a function of temperature. For reference,  $v_T$  is  $7 \text{ m s}^{-1}$  in RE87. When the temperature  $T > 0^\circ\text{C}$ ,  $v_T$  is the calculated value from the warm-rain microphysical scheme:

$$v_T = \begin{cases} 1.0 \text{ m s}^{-1}, & \text{for } -15^\circ\text{C} < T < 0^\circ\text{C}, \\ 0.8 \text{ m s}^{-1}, & \text{for } -35^\circ\text{C} < T < -15^\circ\text{C}, \\ 0.2 \text{ m s}^{-1}, & \text{for } T < -35^\circ\text{C}. \end{cases}$$

The reduced terminal velocities at low temperature increase the residence time of the precipitation and thereby enhance evaporation. The strength of the downdraught is enhanced and a larger horizontal area of moistening and cooling is expected. The latent-heat release of fusion is not considered. Obviously, this method is very primitive.

To simulate large-scale eddy forcing, we add a term to the model's azimuthal momentum equation. For balanced flows, the relevant quantity is the potential-vorticity (PV) flux but, according to the observational study of MV90, the eddy heat fluxes act in the same way as the eddy momentum fluxes, but often with less magnitude and smaller areal coverage. In the present study, we only consider eddy angular-momentum fluxes. We first rewrite the azimuthal momentum equation in RE87 in flux form by using the continuity equation, then divide all physical variables into azimuthal mean and the deviation from the mean, and then average azimuthally again. The new azimuthal

momentum equation takes the following form,

$$\frac{dv}{dt} + \left( f + \frac{v}{r} \right) u = D_v + F_v, \tag{2}$$

where the substantive derivative  $d/dt = \partial/\partial t + u(\partial/\partial r) + w(\partial/\partial z)$ ,  $u$ ,  $v$  and  $w$  are the mean radial, azimuthal, and vertical-velocity components in cylindrical coordinate system  $(r, \phi, z)$  with its axis vertical and  $z$  measuring upward from the surface,  $f$  is assumed constant, and  $D_v$  is the azimuthal mean diffusion.

The term  $F_v$  in Eq. (2) is the azimuthal mean convergence of eddy angular-momentum fluxes. It is here called the ‘eddy spin-up rate’ for convenience. Its form is

$$F_v = \frac{1}{r^2} \frac{\partial}{\partial r} (\overline{-r^2 u' v'}), \tag{3}$$

where the overbar denotes an azimuthal mean and a prime denotes a departure from the mean. Though  $F_v$  has the same mathematical form as the Reynold stresses, it is here assumed to arise from the mutual interaction between a tropical cyclone and its environment. If  $F_v$  is well organized, as discussed by Pfeffer and Challa (1981) and MV90, it can contribute to the initial intensification of a tropical cyclone or could trigger a secondary eyewall. Here  $F_v > 0$  indicates that the eddy exerts a cyclonic torque about the axis and the mean cyclonic angular momentum will increase;  $F_v < 0$  indicates that the eddy exerts an anticyclonic torque about the rotation axis and the mean cyclonic angular momentum will decrease. When  $F_v$  is not equal to zero, there is a transfer of energy between eddy disturbances and the mean field.

Using the observed eddy spin-up rate of MV90 (see their Fig. 7(a)) as guidance, we parametrize  $F_v$  as

$$F_v(r, z, t) = f_v(r) h_v(z) g_v(t), \tag{4}$$

where

$$\begin{aligned} f_v(r) &= \sin \left( 2\pi \frac{r - r_0}{l_r} \right), & r_0 < r < r_0 + l_r, \\ h_v(z) &= \sin \left( \pi \frac{z - z_0}{l_z} \right), & z_0 < z < z_0 + l_z, \\ g_v(t) &= A_{\text{efc}} \exp \left\{ - \left( \frac{t - t_{\text{max}}}{l_t} \right)^2 \right\}. \end{aligned}$$

In the above equations, for the eddy forcing,  $A_{\text{efc}}$  represents the magnitude,  $r_0$  is the starting radius,  $l_r$  is the radial range,  $z_0$  is the starting height,  $l_z$  is the vertical range,  $t_{\text{max}}$  is the peak time and  $l_t$  is the half width of the duration time.

We use the following parameter values:

$$\begin{aligned} A_{\text{efc}} &= 25 \text{ m s}^{-1} \text{ d}^{-1}, \\ r_0 &= 80 \text{ km}, & l_r &= 1600 \text{ km}, \\ z_0 &= 5 \text{ km}, & l_z &= 12 \text{ km}, \\ t_{\text{max}} &= 130 \text{ h}, & l_t &= 30 \text{ h}. \end{aligned}$$

Figure 4 shows the spatial distribution of the eddy spin-up rate at  $t_{\text{max}}$ . Our representation captures major features of the observed eddy forcing. For example, the eddy spin-up rates maximize in the outflow layer, and become negative at large radii.

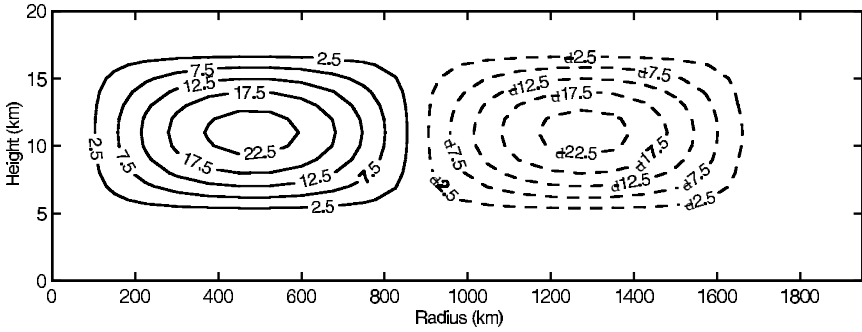


Figure 4. Eddy spin-up rate at  $t = t_{\max}$  used in EXP3. Negative values are dashed. The contour interval is  $5 \text{ m s}^{-1} \text{ d}^{-1}$ .

TABLE 2. DESCRIPTION OF EXPERIMENTS WITH THE FULL-PHYSICS MODEL

EXP1	No eddy forcing is added
EXP2	Same as EXP1 but initial relative humidity is 90% from 1.875 to 9.375 km altitude
EXP3	Same as EXP1 with eddy forcing turned on for 60 h
EXP4	Same as EXP3 but the WISHE mechanism is turned off by using the surface winds at 130 h in the calculations of surface heat fluxes between 130 h and 230 h. After 230 h the WISHE mechanism is switched on again
EXP5	Same as EXP3 but without ice processes
EXP6	Same as EXP3 but no negative spin-up
EXP7	Same as EXP3 but no positive spin-up
EXP8	Same as EXP3 but $A_{\text{efc}} = 15 \text{ m s}^{-1} \text{ d}^{-1}$
EXP9	Same as EXP3 but $A_{\text{efc}} = 35 \text{ m s}^{-1} \text{ d}^{-1}$
EXP10	Same as EXP3 but $A_{\text{efc}} = 35 \text{ m s}^{-1} \text{ d}^{-1}$ but the WISHE mechanism turned off
EXP11	Same as EXP3 but $r_0 = 160 \text{ km}$
EXP12	Same as EXP3 but $r_0 = 300 \text{ km}$
EXP13	Same as EXP3 but $l_r = 1000 \text{ km}$ and $r_b = 3000 \text{ km}$
EXP14	Same as EXP3 but $z_0 = 7 \text{ km}$
EXP15	Same as EXP3 but $l_z = 10 \text{ km}$
EXP16	Same as EXP3 but $t_{\max} = 115 \text{ h}$ , $t_t = 15 \text{ h}$

See text for definition of symbols.

While the observations show no preference for equal areas of cyclonic and anticyclonic spin-up in the radius–height plane, according to Eq. 3,  $\int F_{vr}^2 dr = 0$  must be enforced. Because the model is a closed system, while there is no boundary for a hurricane in nature, the terminating radius of anticyclonic torque is somewhat arbitrarily chosen. Some experiments will be carried out in the next section to test the sensitivity to our chosen parameter values.

(b) Numerical experiments and results

In this section, we present the results of sixteen experiments, which are described in Table 2. We discuss the results for the first four experiments in detail, and list the results of the remaining experiments at the end of this section.

All experiments start with a horizontally uniform sounding and a cyclonic vortex identical to that of the control run of RE87. The initial sounding is neutral to convection in the model atmosphere. The vortex’s maximum tangential wind, radius of maximum tangential wind and radius at which the tangential wind vanishes are  $15 \text{ m s}^{-1}$ ,  $86.25 \text{ km}$  and  $416.25 \text{ km}$ , respectively. The sea surface temperature is  $300 \text{ K}$ , the Coriolis parameter is  $5 \times 10^{-5} \text{ s}^{-1}$ , and the transfer coefficients for momentum and heat (sensible and latent) are equal to  $1.5 \times 10^{-3}$ .

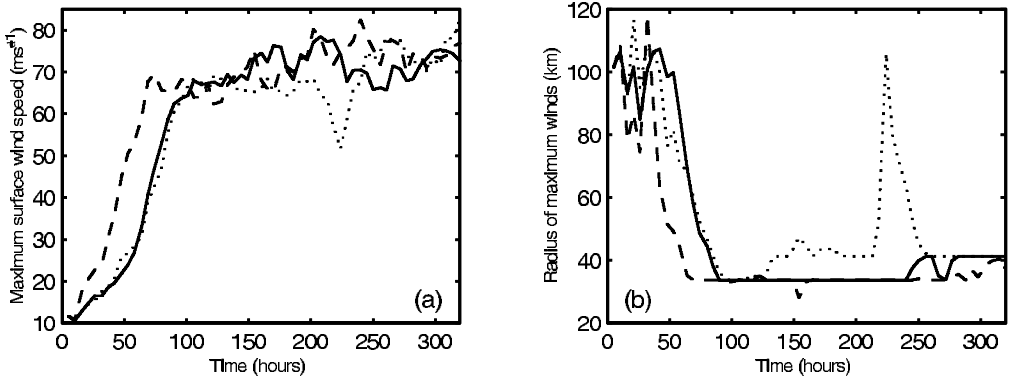


Figure 5. Time evolution of (a) maximum azimuthal surface wind and (b) radius of maximum wind, of EXP1 (solid line), EXP2 (dashed line), and EXP3 (dotted line).

In all experiments, the horizontal and vertical resolutions are 7.5 km and 1.25 km, respectively. The default value of the model outer-wall radius,  $r_b$ , is 2250 km, and the top of the model is at 30 km. A time step of 10 s is used for advective and diffusive processes, while a smaller time step of 2 s is used for computations of the terms associated with sound waves. The total simulation time is 320 h.

Figure 5 displays time series of  $v_{\max}$  and  $r_{\max}$  of EXP1, EXP2 and EXP3.

In the control run EXP1 there is no eddy forcing. It can be seen that the initial cyclonic vortex develops into a hurricane-intensity vortex and reaches statistical equilibrium after 100 h (Fig. 1). The development of  $v_{\max}$  and  $r_{\max}$  is smooth throughout the whole simulation. An eyewall appears around 40 h, and then propagates inwards as it develops over the next 55 h. The eyewall reaches its final position at around 95 h. Only one eyewall forms during the experiment. Due to local conditional instability, deep convective elements occur in the outer region. They are not associated with any local wind maximum, and their average life time is less than between 5 and 10 h. The occasional occurrence of deep convection in the outer region may be responsible for the small fluctuations of  $v_{\max}$  after 100 h.

The time series of  $v_{\max}$  and  $r_{\max}$  from EXP2 (Fig. 5), in which the initial moisture content is increased in the troposphere, indicate that there is no significant intensity change in this experiment. As in EXP1, only one eyewall appears during the experiment. This result contradicts what we found with the simple model. After checking the numerical results in detail, we found two features that may be responsible for the absence of eyewall replacement cycles. First, the initial moisture anomaly added in experiment EXP2 is almost depleted in the first 48 h, owing to precipitation and subsidence in the outer region. The mid-tropospheric entropy thus declines over the first 48 h. The quick loss of the moisture dries the mid-troposphere and thus suppresses the development of small disturbance. In the simple model, however, the mid-tropospheric entropy stays at the higher values during the integration. This is because the crude vertical discretization of the simple model does not permit much subsidence drying of the middle troposphere. Second, there is a strong and persistent low-level temperature inversion layer from 70 to 600 km radius, where the first appearance of a secondary eyewall is usually observed. In the control run of RE87, a similar inversion layer is found (Figs. 5(d) and 8 of RE87). The strong inversion layer suppresses deep convection. The assumption of moist adiabatic lapse rates prevents such an inversion in the simple model.

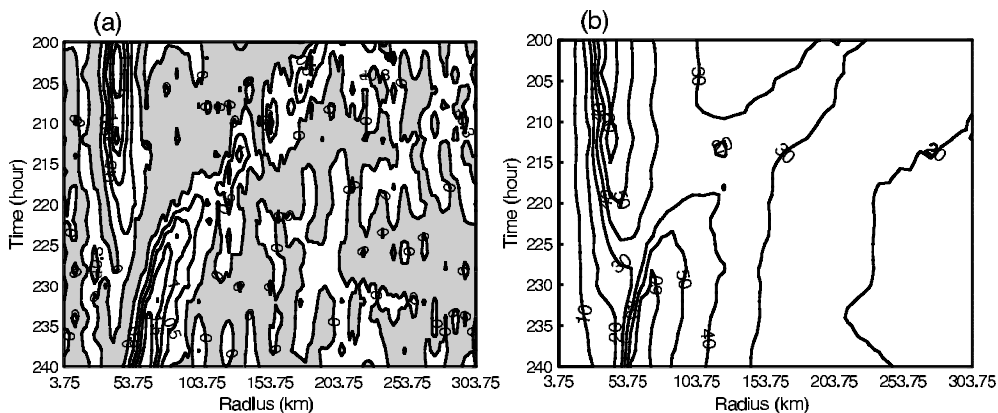


Figure 6. Radius–time plots of (a) vertical velocity at 1250 m and (b) azimuthal velocity at 625 m, of EXP3 between 200 and 240 h. Negative area is shaded. Contour values in (a) are from  $-0.9$  to  $0$  at  $0.3 \text{ m s}^{-1}$  interval and from  $0$  to  $2.5$  at  $0.5 \text{ m s}^{-1}$  interval. Contour values in (b) are from  $10$  to  $70$  at  $10 \text{ m s}^{-1}$  interval.

In EXP3, eddy-flux forcing is turned on for 60 h, peaking at 130 h. The time series of  $v_{\max}$  and  $r_{\max}$  of EXP3 are shown in Fig. 5. There is substantial variation of the model hurricane intensity. Specifically, between 200 and 220 h,  $v_{\max}$  decreases; after 220 h, it increases again. At the turning point at 220 h,  $r_{\max}$  jumps from 40 km to about 120 km, representing an eyewall replacement.

Figure 6 presents radius vs. time plots of vertical velocity at 1250 m and azimuthal velocity at 625 m between 200 and 240 h. Figure 6 clearly depicts a complete eyewall replacement cycle. At 200 h, there are two distinguishable rainbands (or regions of concentrated upward motion) (Fig. 6(a)). Each rainband has its own surface tangential wind maximum (Fig. 6(b)). The one located about 40 km from the centre is the primary eyewall. It is well organized and fully developed, having formed and developed with the spin-up of the initial vortex. The outer rainband around 200 km radius (Fig. 6(a)) is the secondary eyewall, whose vertical kinematic structure is displayed in Fig. 7. The vertical structure of the primary eyewall can also be seen in Fig. 7. Both eyewalls have their own in-up-out secondary circulations and surface tangential wind maxima, consistent with what Samsury and Zipser (1995) found in their flight-level data analysis.

With time (Fig. 6), the outer eyewall contracts and intensifies, while the inner one weakens and dissipates. After the outer eyewall replaces the inner one at 120 km radius around 220 h, the outer eyewall continues to propagate inwards and becomes more intense until it reaches its final position, which is also around 40 km radius. The above eyewall replacement picture is similar to the classical picture described by WCS82. The secondary eyewall in the model has the same kinematic structure as its real-world counterpart.

Figure 8 shows the evolution of  $v_{\max}$  and  $r_{\max}$  in EXP4 and EXP5. EXP4 is the same as EXP3 except that we use the surface wind at 130 h to calculate surface heat and moisture fluxes between 130 and 230 h, and after 230 h we switch back to the normal way of calculating the surface fluxes. As in EXP1 and EXP2, there are no eyewall cycles in this experiment. Thus, as in the simple model, WISHE is essential for concentric eyewalls.

Table 3 summarizes the results of the remaining experiments.

### (c) Discussion of numerical results

Here we describe our understanding of the mechanism responsible for the formation of concentric eyewall cycles in the model.

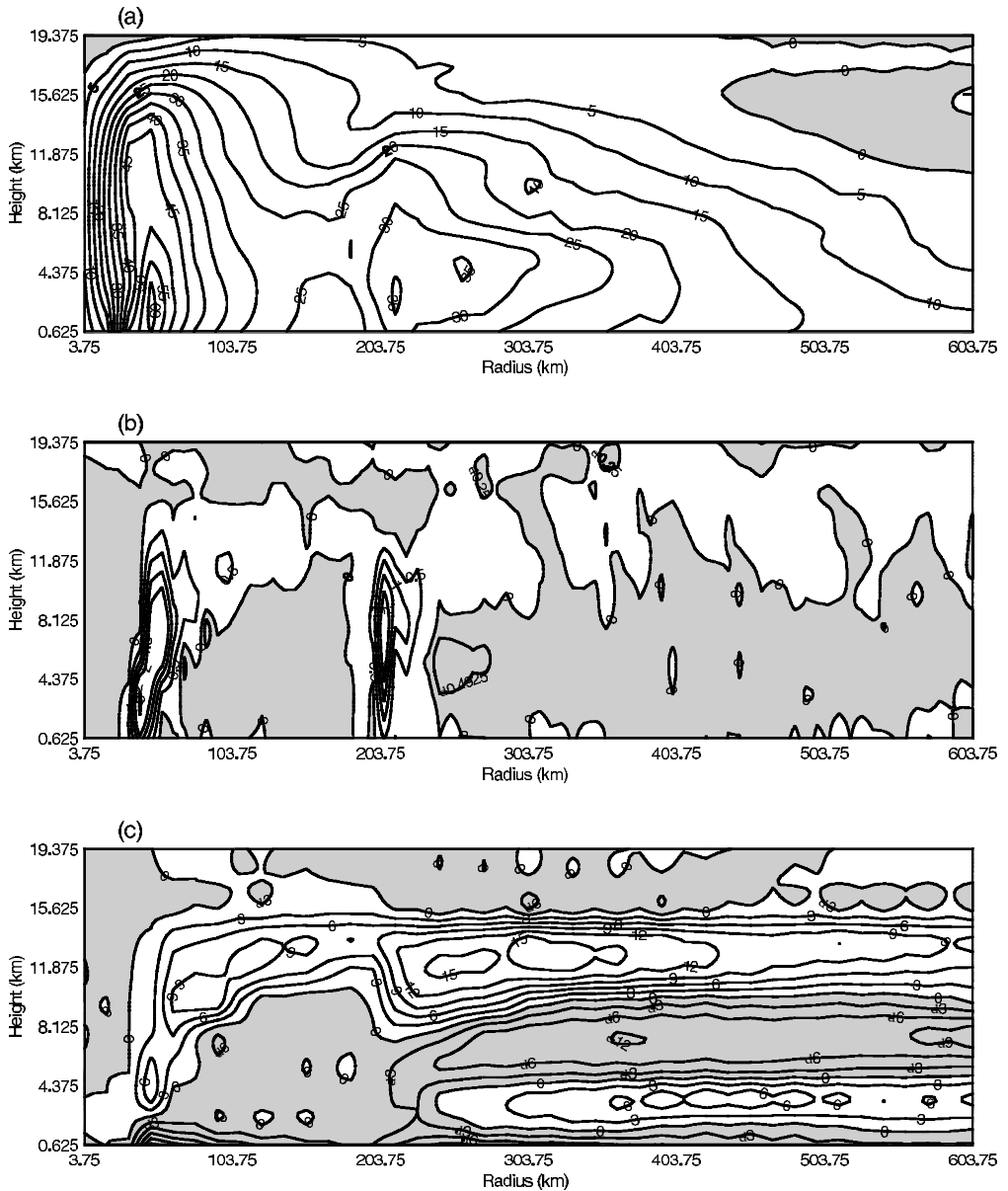


Figure 7. Five-hour averaged values from EXP3 at 200 h: (a) tangential velocity, contour values from  $-5$  to  $70$  at  $5 \text{ m s}^{-1}$  interval; (b) vertical velocity, contour values from  $-0.5$  to  $0$  at  $0.25 \text{ m s}^{-1}$  interval and from  $0$  to  $3.5$  at  $0.5 \text{ m s}^{-1}$  interval; (c) radial velocity, contour values from  $-18$  to  $18$  at  $3 \text{ m s}^{-1}$  interval. Negative areas are shaded throughout.

The WISHE mechanism plays an important role in the amplification of initial wind disturbances. A careful examination of the numerical results, such as vertical velocities of EXP3 and EXP4, reveals that deep convection occurs more frequently within  $600 \text{ km}$  radius in EXP3 than in EXP4. But it is not organized until a substantial surface tangential-wind maximum first appears around  $160 \text{ h}$  at a radius of  $350 \text{ km}$ . With time, this wind maximum evolves into the secondary horizontal wind maximum (SHWM) seen in Fig. 7(a). A strong enough surface wind disturbance can generate

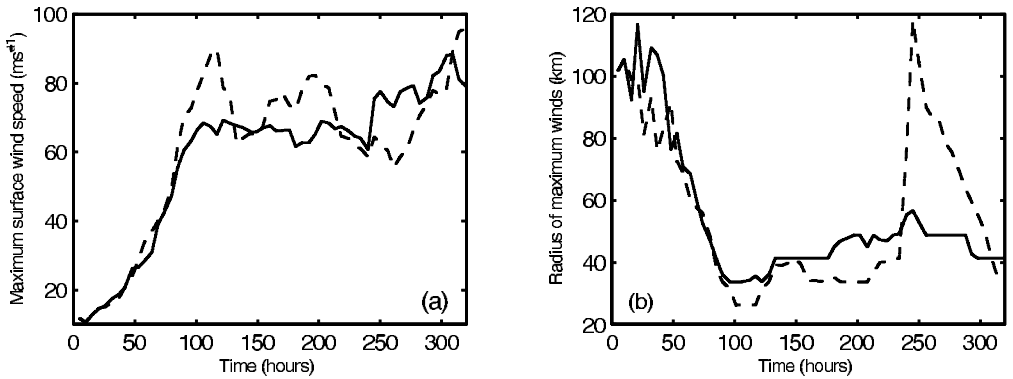


Figure 8. Time evolution of (a) maximum azimuthal surface wind and (b) radius of maximum wind of EXP4 (solid line) and EXP5 (dashed line).

TABLE 3. OBSERVATION OF THE SENSITIVITY EXPERIMENTS

EXP5	Concentric eyewalls form about 40 h later than in EXP3
EXP6	Concentric eyewalls form. The intensity change associated with the eyewall replacement is more pronounced than in EXP3
EXP7	No concentric eyewalls form
EXP8	No concentric eyewalls form
EXP9	Multiple eyewall replacement cycles are found
EXP10	No concentric eyewalls form
EXP11	Concentric eyewalls form. The timing and the magnitude of the intensity change is similar to those of EXP3
EXP12	No concentric eyewalls form
EXP13	No concentric eyewalls form
EXP14	No concentric eyewalls form
EXP15	No concentric eyewalls form
EXP16	No concentric eyewalls form

sufficient moist entropy fluxes from the ocean surface to the subcloud layer to counteract the depletion of subcloud-layer entropy by the evaporatively driven downdraughts, so that the disturbance is eventually amplified by the WISHE mechanism, as seen in Fig. 6. Furthermore, numerical results from EXP4 demonstrate that without WISHE there is no genesis of a secondary eyewall in the full-physics model. This result agrees with what we found using the simple model.

Evaporatively driven downdraughts and ice processes also play some role in the development of the initial weak SHWM. It should be kept in mind that no real ice scheme has been implemented in the model. It is seen in Fig. 7(b) that a significant branch of convective downdraughts exists next to the secondary eyewall away from the storm centre. The downdraughts originate at about 5–6 km height where  $T < 0^{\circ}\text{C}$ . The downdraughts remain active until the secondary eyewall has replaced the primary one completely and reaches its final position. In our primitive ice scheme, there is extra evaporation of the precipitation when  $T < 0^{\circ}\text{C}$ , owing to its slow fall speed. The extra evaporation results in extra cooling, enhancing the existing downdraughts. The occurrence of the downdraughts, through mass continuity, leads to mid- to upper-level inflow (Fig. 7(c)). This radial inflow brings relatively low-entropy and high-angular-momentum middle-tropospheric air towards the outer edge of the secondary eyewall, which will also increase evaporation and the cyclonic rotation tendency there. Both increases in the evaporation will further enhance the convective downdraughts. Most of the cyclonic tendency is transported down to the surface by the downdraughts.

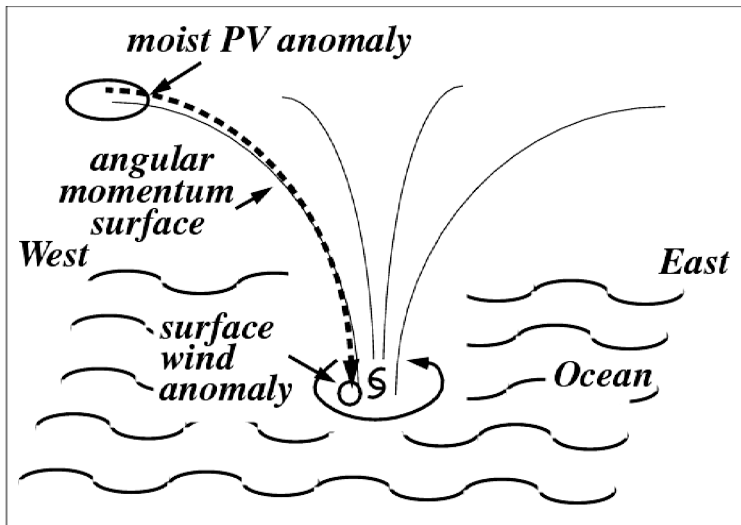


Figure 9. Schematic illustration of how an upper-level moist PV anomaly induces a surface wind anomaly. The arrow from upper troposphere to surface indicates that the PV anomaly projects a cyclonic component downwards along the angular-momentum surface to the ocean surface.

The SHWM will then be further enhanced, as will the surface heat fluxes. This is probably the reason that the vortex is a little stronger after the eyewall replacement (see dotted lines in Fig. 5). The other role of the downdraughts is to transport low-entropy air into the subcloud layer, which prevents new deep convection from occurring near the secondary eyewall. This process keeps the latent-heat release in a small area (at least not outside the secondary eyewall). This means that the heating can more efficiently maintain, or even increase, the existing horizontal temperature gradient associated with the secondary eyewall at upper levels, strengthening the SHWM. Thus, convective downdraughts may help maintain and develop the SHWM. The effect of ice processes is achieved indirectly through enhancing the downdraughts.

To further assess the importance of ice processes, we perform EXP5 in which the ice processes are turned off. The time series of  $v_{\max}$  and  $r_{\max}$  are presented in Fig. 8. As seen in Fig. 8, the secondary eyewall appears about 40 h later than in EXP3. Except for this late appearance, the process of the formation of the secondary eyewall is very similar to that in EXP3.

Given the potential importance of the surface wind anomaly, we inquire about the origin of the initial wind anomaly. With the aid of Fig. 9, we employ 'PV thinking' to tackle this question. Following Hoskins *et al.* (1985), given distributions of global PV and state variables such as potential temperature at lower boundaries, one can deduce the distributions of mass and wind speeds under a suitable balance condition. In the moist atmosphere, instead of using conventional PV defined in the paper of Hoskins *et al.* (1985), we use the saturated moist PV\*. Since the saturated moist PV is nearly zero in a hurricane (e.g. see RE87),  $\theta_e^*$  is invariant along angular-momentum surfaces, which act as characteristic surfaces in saturated moist PV inversion. When an upper-level trough is located several hundred kilometres to the west and polewards of a hurricane, the

\* Saturated moist PV,  $q_e^* \equiv (1/\rho)(\boldsymbol{\eta} \cdot \nabla\theta_e^*)$ , where  $\boldsymbol{\eta}$  is the absolute vorticity,  $\rho$  is the air density, and  $\theta_e^*$  is the saturated equivalent potential temperature. Note that since  $\theta_e^*$  is a state variable,  $q_e^*$  is fully invertible, unlike the quantity  $q_e \equiv (1/\rho)(\boldsymbol{\eta} \cdot \nabla\theta_e)$ , where  $\theta_e$  is the moist potential temperature.

trough begins to interact with the hurricane. As is usually done in studying midlatitude dynamics, the trough can be thought of as an upper-level moist PV anomaly, as shown in Fig. 9. Through this interaction, the cyclonic vorticity associated with the trough projects along angular-momentum surfaces down to the ocean surface to produce a surface wind anomaly. This argument was first suggested by Emanuel (1997). Indeed, MV90 observed downward and inward shifting of the maximum spin-up rate from 200 to 900 mb (see their Fig. 7). Once a wind anomaly forms at the surface, it may develop into a secondary eyewall through the WISHE mechanism, given favourable conditions.

Finally, our sensitivity tests (Table 3) show that the eddy forcing should be present long enough, be close enough to the vortex centre and the surface, and be broad enough horizontally and vertically. Our numerical results are in agreement with Holland's (1987) suggestion that eddy forcing should reach inward of a critical radius in order to interact with the storm's inner core. By trial and error, we found that the threshold value for  $A_{\text{efc}}$  to produce concentric eyewall cycles under the conditions of experiment EXP3 is  $19 \text{ m s}^{-1} \text{ d}^{-1}$ . The critical strength of the eddy forcing is, of course, a function of initial conditions and parameter values of the non-hydrostatic model.

#### (d) *Conclusions from the non-hydrostatic model*

Based on the numerical experiments with the non-hydrostatic model, we draw the following conclusions:

- (i) The model does not spontaneously produce concentric eyewalls, even when the initial humidity of the middle troposphere is increased. This is probably because of two adverse factors: the quick loss of initial moisture through precipitation, and the formation of a strong temperature inversion above the boundary layer and stretching from the eyewall to about 600 km, where the observed concentric eyewalls usually form in the real world. The presence of the inversion and the quick depletion of the initial moisture suggest that only finite-amplitude perturbations can trigger concentric eyewall cycles in the model. This is consistent with the conclusion based on the randomized numerical experiments EX4 and EX5 described in section 2(b).
- (ii) After an external forcing of sufficient amplitude and spatial and temporal extent is introduced at upper levels, the model produces concentric eyewalls. The external forcing induces a wind disturbance at the sea surface through the projection of an upper-level moist PV anomaly downwards along angular-momentum surfaces, which act as characteristic surfaces under saturated moist PV inversion (Emanuel 1997).
- (iii) This initial disturbance may develop into a SHWM under the influence of evaporatively driven downdraughts and ice microphysical processes, which enhance the strength of the downdraughts. When the SHWM becomes strong enough, it triggers the formation of a secondary eyewall through the WISHE mechanism.
- (iv) The concentric eyewall cycles in the model have characteristics similar to those in nature; for example, their kinematic structure and intensity change are similar.

#### 4. FINAL REMARKS

We used two numerical models in an attempt to understand the dynamics of the genesis of concentric eyewalls in hurricanes. We specifically focused on the effects of the WISHE mechanism and the external eddy forcing associated with upper-level wave asymmetries in the environment of tropical cyclones.

We draw the following conclusions, with some caveats:

(i) The numerical simulations suggest that the WISHE mechanism plays a critical role in the development of outer wind maxima. The foundation of this mechanism is the augmentation of wind-speed-dependent sea-to-air enthalpy transfer above ambient values. Such wind-speed-dependent transfer makes possible a positive feedback between an intense vortex-scale flow and the surface fluxes. The importance of this feedback has been borne out convincingly by numerical experiments in which WISHE is turned off. No disturbance in either model can develop outside the primary eyewall without this positive feedback.

(ii) Randomized experiments with the simple model suggest that, unless the middle troposphere is very moist, a sufficiently strong external disturbance is necessary for the formation of a secondary eyewall, which is in accord with the finite-amplitude nature of tropical cyclogenesis. This is because precipitation-induced downdraughts stabilize the outer region by depleting subcloud-layer entropy. This effect is crucial to the development and maintenance of a tropical cyclone, but it is detrimental to the genesis of concentric eyewalls. However, if the lower and middle troposphere are moist enough in the simple model, the cooling effect of the downdraughts is reduced to the point that disturbances can develop.

The non-hydrostatic model, however, does not spontaneously produce concentric eyewalls, even when the initial moisture in the troposphere is increased. Two features may be responsible for this: the relatively quick reduction of the initial moisture anomaly owing to subsidence, and a noticeable temperature inversion above the boundary layer in the outer region. The overall effect of these features is to stabilize the primary eyewall, while suppressing small perturbations.

In brief, results from both models suggest that the genesis of concentric eyewall hurricane results from a finite-amplitude WISHE instability of tropical cyclones.

(iii) Where do the initial finite-amplitude perturbations that trigger the concentric eyewall cycles come from? We propose that the perturbations are induced by external factors, for example, tropospheric and lower-stratospheric environmental forcing.

We hypothesize, as illustrated in Fig. 9, that when an upper-level trough approaches to within several hundred kilometers of the centre of a hurricane, as argued by Emanuel (1997), the cyclonic vorticity associated with the trough may project downwards to the surface along angular-momentum surfaces, which function as characteristic surfaces in saturated moist PV inversion. Once a local surface wind maximum forms, it amplifies through the WISHE mechanism. Our sensitivity tests show that the external forcing must last long enough, be close to the vortex centre, and be broad enough in space. This external forcing acts as a catalyst for the finite-amplitude WISHE.

In future work, we will present an analysis of the synoptic environment of 22 concentric eyewall hurricanes and one non-concentric eyewall hurricane.

#### ACKNOWLEDGEMENT

This research was supported by the National Science Foundation, under Grant ATM-9708322.

#### REFERENCES

- |                                    |      |                                                                                                                         |
|------------------------------------|------|-------------------------------------------------------------------------------------------------------------------------|
| Bister, M.                         | 1996 | 'Development of tropical cyclones from mesoscale convective systems'. PhD thesis, Massachusetts Institute of Technology |
| Black, M. L. and Willoughby, H. E. | 1992 | The concentric eyewall cycle of Hurricane Gilbert. <i>Mon. Weather Rev.</i> , <b>120</b> , 947–957                      |

- Camp, J. P. and Montgomery, M. T. 2001 Hurricane maximum intensity: Past and present. *Mon. Weather Rev.*, **129**, 1704–1717
- Craig, G. C. 1996 Numerical experiments on radiation and tropical cyclones. *Q. J. R. Meteorol. Soc.*, **122**, 415–422
- DeMaria, M., Baik, J. J. and Kaplan, J. 1993 Upper-level eddy angular momentum fluxes and tropical cyclone intensity change. *J. Atmos. Sci.*, **50**, 1133–1147
- Emanuel, K. A. 1989 The finite-amplitude nature of tropical cyclogenesis. *J. Atmos. Sci.*, **46**, 3431–3456
- 1993 The effects of convective response time on WISHE modes. *J. Atmos. Sci.*, **50**, 1763–1775
- 1995 The behavior of a simple hurricane model using a convective scheme based on subcloud-layer entropy equilibrium. *J. Atmos. Sci.*, **52**, 3960–3968
- 1997 Some aspects of hurricane inner-core dynamics and energetics. *J. Atmos. Sci.*, **54**, 1014–1026
- Hawkins, H. F. 1983 Hurricane Allen and island obstacles. *J. Atmos. Sci.*, **40**, 1360–1361
- Holland, G. J. 1987 ‘Mature structure and structure change’. Pp. 13–52 in *A global view of tropical cyclones*. Ed. R. L. Elsberry. Naval Postgraduate School, Monterey, CA, USA
- Hoskins, B. J., McIntyre, M. E. and Robertson, A. W. 1985 On the use and significance of isentropic potential-vorticity maps. *Q. J. R. Meteorol. Soc.*, **111**, 877–916
- Lord, S. J., Willoughby, H. E. and Piotrowicz, J. M. 1984 Role of a parametrized ice-phase microphysics in an axisymmetric, non-hydrostatic tropical cyclone model. *J. Atmos. Sci.*, **41**, 2836–2848
- Molinari, J. and Vollaro, D. 1989 External influences on hurricane intensity. Part I: Outflow-layer eddy angular momentum fluxes. *J. Atmos. Sci.*, **46**, 1093–1105
- 1990 External influences on hurricane intensity. Part II: Vertical structure and response of the hurricane vortex. *J. Atmos. Sci.*, **47**, 1902–1918
- 1992 ‘Environmental controls on eye wall cycles and intensity change in Hurricane Allen (1980)’. Pp. 328–337 in *Tropical cyclone disasters*. Eds. J. Lighthill, Z. Zheming, G. Holland and K. Emanuel. Peking University Press, Beijing, P.R. China
- Molinari, J., Skubis, S. and Vollaro, D. 1995 External influences on hurricane intensity. Part III: Potential vorticity structure. *J. Atmos. Sci.*, **52**, 3593–3606
- Montgomery, M. T. and Kallenbach, R. J. 1997 A theory for vortex Rossby waves and its application to spiral bands and intensity changes in hurricanes. *Q. J. R. Meteorol. Soc.*, **123**, 435–465
- Pfeffer, R. L. and Challa, M. 1981 A numerical study of the role of eddy fluxes of momentum in the development of Atlantic hurricanes. *J. Atmos. Sci.*, **38**, 2393–2398
- Riehl, H. 1979 *Climate and weather in the Tropics*. Academic Press, New York
- Rotunno, R. and Emanuel, K. A. 1987 An air–sea interaction theory for tropical cyclones. Part II: Evolutionary study using a nonhydrostatic axisymmetric numerical model. *J. Atmos. Sci.*, **44**, 542–561
- Samsury, C. E. and Zipser, E. J. 1995 Secondary wind maxima in hurricane: Airflow and relationship to rainbands. *Mon. Weather Rev.*, **123**, 3502–3517
- Shapiro, L. J. and Willoughby, H. E. 1982 The response of balanced hurricanes to local sources of heat and momentum. *J. Atmos. Sci.*, **39**, 378–394
- Willoughby, H. E. 1988 The dynamics of the tropical cyclone core. *Aust. Meteorol. Mag.*, **36**, 183–191
- 1990 Temporal changes of the primary circulation in tropical cyclones. *J. Atmos. Sci.*, **47**, 242–264
- Willoughby, H. E. and Black, P. G. 1996 Hurricane Andrew in Florida: Dynamics of a disaster. *Bull. Am. Meteorol. Soc.*, **77**, 543–549
- Willoughby, H. E., Clos, J. A. and Shoreibah, M. G. 1982 Concentric eye walls secondary wind maxima, and the evolution of the hurricane vortex. *J. Atmos. Sci.*, **39**, 395–411
- Willoughby, H. E., Jin, H.-L., Lord, S. J. and Piotrowicz, J. M. 1984 Hurricane structure and evolution as simulated by an axisymmetric, non-hydrostatic numerical model. *J. Atmos. Sci.*, **41**, 1169–1186